ELSEVIER

SCIENCE DIRECT

Physics Letters B 605 (2005) 115–122

PHYSICS LETTERS B

www.elsevier.com/locate/physletb

pp elastic scattering at LHC in near forward direction

M.M. Islam [a], R.J. Luddy [a], A.V. Prokudin [b,c,d]

[a] *Department of Physics, University of Connecticut, Storrs, CT 06269, USA*
[b] *Dipartmento di Fisica Teorica, Università Degli Studi di Torino, Via Pietro Giuria 1, 10125 Torino, Italy*
[c] *Sezione INFN di Torino, Italy*
[d] *Institute for High Energy Physics, 142281 Protvino, Russia*

Received 28 September 2004; received in revised form 29 October 2004; accepted 2 November 2004

Available online 12 November 2004

Editor: G.F. Giudice

Abstract

We predict pp elastic differential cross section at LHC at the c.m. energy $\sqrt{s} = 14$ TeV and momentum transfer range $|t| =$ 0–10 GeV^2, which is planned to be measured by the TOTEM group. The field theory model underlying our phenomenological investigation describes the nucleon as a composite object with an outer cloud of quark–antiquark condensate, an inner core of topological baryonic charge, and a still smaller quark-bag of valence quarks. The model satisfactorily describes the asymptotic behavior of $\sigma_{\rm tot}(s)$ and $\rho(s)$ as well as the measured $\bar{p}p$ elastic $d\sigma/dt$ at $\sqrt{s} = 546$ GeV, 630 GeV, and 1.8 TeV. The large $|t|$ elastic amplitude of the model incorporates the BFKL pomeron in next to leading order approximation, the perturbative dimensional counting behavior, and the confinement of valence quarks in a small region within the nucleon.

PACS: 12.39.-x; 13.85.Dz; 14.20.Dh

Keywords: pp scattering; LHC/TOTEM; Nucleon structure; Hard pomeron

pp elastic differential cross section at LHC in near forward direction at c.m. energy $\sqrt{s} = 14$ TeV and momentum transfer $|t| = 0$–10 GeV^2 is planned to be measured by the TOTEM (TOTal and Elastic Measurement) group [1]. Various models have been proposed to describe pp elastic scattering in the diffraction region $|t| \simeq 0$–0.5 GeV^2, such as: (i) single pomeron exchange with a trajectory $\alpha_P(t) = 1.08 + 0.25t$ [2], (ii) multiple pomeron exchanges with single- and double-diffractive dissociation [3], (iii) the incident proton viewed as made-up of two color dipoles in the target proton rest frame [4]. pp elastic $d\sigma/dt$ at LHC all the way from $|t| = 0$ to 10 GeV^2 has been predicted on the basis of three different models: (a) impact-picture model [5] based on the Cheng–Wu calculation

E-mail addresses: islam@phys.uconn.edu (M.M. Islam), rjluddy@phys.uconn.edu (R.J. Luddy), prokudin@to.infn.it (A.V. Prokudin).

0370-2693
doi:10.1016/j.physletb.2004.11.006

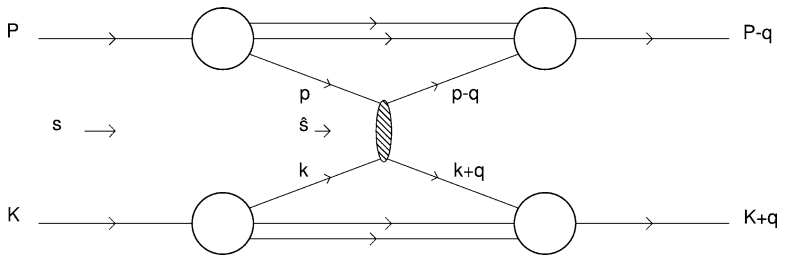

Fig. 1. Hard collision of valence quarks from two different protons.

of QED tower diagrams [6], (b) eikonalized pomeron–reggeon model using conventional Regge approach, but with multiple pomeron–reggeon exchanges included [7,8], (c) effective field theory model that describes the nucleon as a chiral-bag with a quark–antiquark cloud [9,10]. A QCD-inspired eikonalized model has also been proposed to predict pp $d\sigma/dt$ at $\sqrt{s} = 14$ TeV for $|t| = 0$–2.0 GeV^2 [11]. This wide array of models attempting to describe pp elastic scattering at LHC reflects the view that quantitative understanding of this process will provide fundamental insight into the nonperturbative and the perturbative QCD dynamics.

The impact-picture model and the eikonalized pomeron–reggeon model predict besides the first dip-bump structure more diffraction-like secondary structures at large $|t|$ [5,7,8]. The chiral-bag model with $q\bar{q}$ condensate cloud, which we studied [9], predicts after the first dip-bump structure a smooth approximately exponential fall-off (known as Orear fall-off) and then a slower fall-off due to the transition from the nonperturbative regime to the perturbative regime. This change in the behavior of $d\sigma/dt$ was shown only schematically in our previous work [9]. We have now been able to quantitatively address this question and study the predicted change of $d\sigma/dt$. Results of our investigation and the implications for the combined role of perturbative and nonperturbative QCD dynamics are briefly reported here.

We view pp elastic scattering in the perturbative regime as a hard collision of a valence quark from one proton with a valence quark from the other proton (Fig. 1). The collision carries off the whole momentum transfer. This dynamical picture brings new features in our calculations: (1) probability amplitude of a quark to have, say, momentum $\vec{p}$ when the proton has momentum $\vec{P}$ in the c.m. frame. (2) Quark–quark elastic amplitude at high energy and large momentum transfer, which is in the domain of perturbative QCD. The latter has been the focus of extensive studies following the original work of Balitsky, Fadin, Kuraev, and Lipatov (BFKL) [12]. The present status is that the qq elastic scattering occurs via reggeized gluon ladders with rungs of gluons which represent gluon emissions in inelastic processes (BFKL pomeron). It is a crossing-even amplitude which is a cut in the angular momentum plane with a fixed branch point at $\alpha_{\mathrm{BFKL}} = 1 + \omega$. The value of ω in the next-to-leading order (NLO) lies in the range 0.13–0.18 as argued by Brodsky et al. [13]. We refer to the BFKL pomeron with next to leading order corrections included as the QCD "hard pomeron". In our investigation, we approximate this hard pomeron by a fixed pole and take the qq scattering in Fig. 1 as

$$\hat{T}(\hat{s},t) = i\gamma_{qq}\hat{s}\left(\hat{s}e^{-i\frac{\pi}{2}}\right)^{\omega}\frac{1}{|t| + r_0^{-2}}, \tag{1}$$

where $\hat{s} = (p+k)^2$, $t = -\vec{q}^{\,2}$. The phase in Eq. (1) follows from the requirement that $\hat{T}(\hat{s},t)$ is a crossing even amplitude. Eq. (1) represents the hard pomeron amplitude in our calculations. If we want to describe just asymptotic qq scattering, we have to take into account unitarity corrections due to infinite exchanges of this pomeron. This can be done by taking $\hat{T}(\hat{s},t)$ as the Born amplitude in an eikonal formulation [14], which leads to a black-disk description and requires $\gamma_{qq} > 0$. The radius of the black disk turns out to be $R(\hat{s}) = r_0\omega\ln\hat{s}$. Hence, the parameter r_0 in Eq. (1) has the physical significance of a length scale that defines the black-disk radius of asymptotic quark–quark scattering.

We next examine how to obtain the pp elastic scattering amplitude from the process shown in Fig. 1. Let s be the square of the c.m. energy of the two collid-

ing protons: $s = (P + K)^2$. $\hat{s}$, of course, is the square of the c.m. energy of the two colliding quarks. From Fig. 1, we see that initially we have a quark of momentum $\vec{p}$: $|\vec{p}\rangle$ with a probability amplitude $\varphi(\vec{p})$ in the c.m. frame in which the proton is moving with momentum $\vec{P}$. Similarly, we have a second quark with momentum $\vec{k}$: $|\vec{k}\rangle$ with a probability amplitude $\varphi(\vec{k})$ in the c.m. frame in which the other proton is moving with momentum $\vec{K} = -\vec{P}$. Thus, the initial state of the two colliding quarks is

$$|i\rangle = \varphi(\vec{p})|\vec{p}\rangle\varphi(\vec{k})|\vec{k}\rangle. \tag{2}$$

After the collision, we have a quark with momentum $\vec{p} - \vec{q}$: $|\vec{p} - \vec{q}\rangle$ with a probability amplitude $\varphi(\vec{p} - \vec{q})$, and a quark with momentum $\vec{k} + \vec{q}$: $|\vec{k} + \vec{q}\rangle$ with a probability amplitude $\varphi(\vec{k} + \vec{q})$. So, the final state is

$$|f\rangle = \varphi(\vec{p} - \vec{q})|\vec{p} - \vec{q}\rangle\varphi(\vec{k} + \vec{q})|\vec{k} + \vec{q}\rangle. \tag{3}$$

The pp elastic scattering amplitude due to quark–quark scattering $T_{qq}(s, -\vec{q}^{\,2})$ from Fig. 1 is then

$$T_{qq}\big(s, -\vec{q}^{\,2}\big) = \sum_{\vec{p}}\sum_{\vec{k}} \varphi^*(\vec{p} - \vec{q})\varphi^*(\vec{k} + \vec{q}) \times \langle \vec{k} + \vec{q}|\langle \vec{p} - \vec{q}|\hat{T}_{\rm op}|\vec{p}\rangle|\vec{k}\rangle\varphi(\vec{p})\varphi(\vec{k}), \tag{4}$$

where $\langle \vec{k} + \vec{q}|\langle \vec{p} - \vec{q}|\hat{T}_{\rm op}|\vec{p}\rangle|\vec{k}\rangle$ is the qq elastic scattering amplitude. Since this amplitude only depends on the invariants $\hat{s} = (p + q)^2$ and $\hat{t} = -\vec{q}^{\,2}$, we can write

$$\langle \vec{k} + \vec{q}|\langle \vec{p} - \vec{q}|\hat{T}_{\rm op}|\vec{p}\rangle|\vec{k}\rangle = \hat{T}\big(\hat{s}, -\vec{q}^{\,2}\big). \tag{5}$$

Eq. (4) then takes the form

$$T_{qq}\big(s, -\vec{q}^{\,2}\big) = \sum_{\vec{p}}\sum_{\vec{k}} \varphi^*(\vec{p} - \vec{q})\varphi(\vec{p})\hat{T}\big(\hat{s}, -\vec{q}^{\,2}\big) \times \varphi^*(\vec{k} + \vec{q})\varphi(\vec{k}). \tag{6}$$

This equation makes it evident that $\varphi^*(\vec{p} - \vec{q})\varphi(\vec{p})$ and $\varphi^*(\vec{k} + \vec{q})\varphi(\vec{k})$ are the nonperturbative "impact factors" which modify the perturbative qq amplitude $\hat{T}(\hat{s}, -\vec{q}^{\,2})$. The right-hand side (RHS) of Eq. (6) needs to be multiplied by a factor of nine to take into account that there are three quarks in each proton.[1] We absorb this factor in the constant γ_{qq}.

[1] The quarks in our field theory model (Ref. [10]) are massless effective color-singlet quarks and not the QCD current quarks.

To see the physical meaning of Eq. (6), let us assume that we can approximate qq scattering in Fig. 1 by taking some average value of $\hat{s}$: $\hat{s}_{\rm av}$. Of course, $\hat{s}_{\rm av}$ is going to be proportional to s. Eq. (6) then takes the form

$$T_{qq}\big(s, -\vec{q}^{\,2}\big) \simeq \sum_{\vec{p}} \varphi^*(\vec{p} - \vec{q})\varphi(\vec{p})\hat{T}\big(\hat{s}_{\rm av}, -\vec{q}^{\,2}\big) \times \sum_{\vec{k}} \varphi^*(\vec{k} + \vec{q})\varphi(\vec{k}), \tag{7}$$

which shows that the impact factors separate out. Each momentum sum in Eq. (7) can now be carried out and yields the form factor associated with the quark probability density in the c.m. frame. This probability density is Lorentz contracted, which means if $\rho_0(\vec{r}\,')$ is the quark probability density at $\vec{r}\,'$ in the proton rest frame and $\rho(\vec{r})$ is the probability density at $\vec{r}$ in the c.m. frame, then

$$\rho(\vec{b} + \vec{e}_3 z) = \gamma\rho_0(\vec{b} + \vec{e}_3\gamma z), \tag{8}$$

where γ is the Lorentz contraction factor: $\gamma = E/M = \sqrt{s}/(2M)$, $\vec{r} = \vec{b} + \vec{e}_3 z$, and $\vec{e}_3$ is the unit vector in the direction of $\vec{P}$, i.e., the z-axis. If $F(\vec{q})$ is the form factor associated with $\rho_0(\vec{r})$:

$$F(\vec{q}) = \int d^3r\, e^{i\vec{q}\cdot\vec{r}}\rho_0(\vec{r}), \tag{9}$$

and $\rho_0(\vec{r})$ is spherically symmetric, then

$$\sum_{\vec{p}} \varphi^*(\vec{p} - \vec{q})\varphi(\vec{p}) = \int d^3r\, e^{-i\vec{q}\cdot\vec{r}}\rho(\vec{r}) = F\left(\vec{q}_\perp + \vec{e}_3\frac{q_3}{\gamma}\right). \tag{10}$$

In deriving Eq. (10), we have used $\rho(\vec{r}) = \psi^*(\vec{r})\psi(\vec{r})$, where the quark wave function $\psi(\vec{r})$ is related to its momentum wave function $\varphi(\vec{p})$ via the plane wave expansion:

$$\psi(\vec{r}) = \sum_{\vec{p}} \frac{e^{i\vec{p}\cdot\vec{r}}}{\sqrt{V}}\varphi(\vec{p}). \tag{11}$$

Eq. (7) now takes the form

$$T_{qq}\big(s, -\vec{q}^{\,2}\big) \simeq F(\vec{q}_\perp)\hat{T}\big(\hat{s}_{\rm av}, -\vec{q}^{\,2}\big)F(\vec{q}_\perp) \quad \left(\frac{q_3}{\gamma} = \frac{2Mq_3}{\sqrt{s}} \to 0\right). \tag{12}$$

The structure of Eq. (12) is easy to understand. It is the usual quantum-mechanical scattering amplitude of two composite objects described by the form factors and interacting via a basic process whose amplitude is $\hat{T}(\hat{s}_{\rm av}, -\vec{q}^{\,2})$. We take the form factor $F(\vec{q})$ describing the quark probability density or number density in the nucleon rest frame to be a dipole:

$$F(\vec{q}) = \left(1 + \frac{\vec{q}^{\,2}}{m_0^2}\right)^{-2}, \tag{13}$$

so that it satisfies the dimensional counting behavior t^{-2} for the form factor of a proton made up of three quarks [15–17].

Now we go back to Eq. (6) and no longer make the approximation of replacing $\hat{s}$ by an average value. $T_{qq}(s, -\vec{q}^{\,2})$ in Eq. (6) represents the pp elastic amplitude that originates from the qq elastic amplitude $\hat{T}(\hat{s}, -\vec{q}^{\,2})$ occurring on the RHS of Eq. (6). The process is depicted in Fig. 1. We take the qq amplitude $\hat{T}(\hat{s}, -\vec{q}^{\,2})$ as due to the hard pomeron given by Eq. (1). Eq. (6), then leads to

$$T_{qq}\big(s, -\vec{q}^{\,2}\big) = \sum_{\vec{p}} \sum_{\vec{k}} \varphi^*(\vec{p} - \vec{q})\varphi(\vec{p}) i\gamma_{qq} \hat{s} \big(\hat{s} e^{-i\frac{\pi}{2}}\big)^{\omega} \times \frac{1}{\vec{q}^{\,2} + r_0^{-2}} \varphi^*(\vec{k} + \vec{q})\varphi(\vec{k}). \tag{14}$$

Introducing light-cone variables $P_+ = P_0 + P_3$, $P_- = P_0 - P_3$, $p_+ = p_0 + p_3$, $p_- = p_0 - p_3$, etc. and writing $p_+ = x P_+$, $k_- = x' K_-$, we find $\hat{s} \simeq x x' s$, when P_+, $K_- \to \infty$. Eq. (14) then takes the separable form

$$T_{qq}\big(s, -\vec{q}^{\,2}\big) = \left(\sum_{\vec{p}} \varphi^*(\vec{p} - \vec{q})\varphi(\vec{p}) x^{1+\omega}\right) i\gamma_{qq} s \big(s e^{-i\frac{\pi}{2}}\big)^{\omega} \times \frac{1}{\vec{q}^{\,2} + r_0^{-2}} \left(\sum_{\vec{k}} \varphi^*(\vec{k} + \vec{q})\varphi(\vec{k}) x'^{1+\omega}\right). \tag{15}$$

In a frame where $P_+ \to \infty$,

$$\sum_{\vec{p}} \varphi^*(\vec{p} - \vec{q})\varphi(\vec{p}) x^{1+\omega} = \frac{M m_0^5}{8\pi} \int_0^1 dx \frac{x^{1+\omega}}{(\frac{m_0^2}{4} + M^2 x^2)} I\big(q_\perp, \alpha(x)\big), \tag{16}$$

where

$$I\big(q_\perp, \alpha(x)\big) \equiv \int_0^\infty b\, db\, J_0(b q_\perp) \big\{b K_1[b\alpha]\big\}^2. \tag{17}$$

Here M is the nucleon mass, m_0 is the mass parameter that occurs in the form factor Eq. (13), $\alpha = (\frac{m_0^2}{4} + M^2 x^2)^{1/2}$, and $\vec{q} \simeq \vec{q}_\perp$. In deriving Eq. (16), we use momentum wave function $\varphi(\vec{p})$ obtained from the Lorentz contracted probability density. It can be related to the rest frame wave function $\varphi_0(\vec{p}')$ in the following way:

$$\varphi(\vec{p}_\perp + \vec{e}_3 p_3) = \varphi_0\left(\vec{p}_\perp + \vec{e}_3 \frac{p_3}{\gamma}\right), \tag{18}$$

and yields the result

$$\varphi(\vec{p}_\perp + \vec{e}_3 p_3) = \left(\frac{2\pi m_0^5}{V_0}\right)^{1/2} \left(\frac{m_0^2}{4} + p_\perp^2 + \frac{p_3^2}{\gamma^2}\right)^{-2}. \tag{19}$$

(V_0 is the quantization volume in the rest frame.) The integral $I(q_\perp, \alpha(x))$ can be evaluated analytically, and we obtain

$$I\big(q_\perp, \alpha(x)\big) = \frac{1}{8\alpha^4}\left\{\frac{2}{a^3 a'} \ln(a' + a) + \frac{1}{a a'^3} \ln(a' + a) - \frac{1}{a^2 a'^2} - \frac{3a'}{a^5} \ln(a' + a) + \frac{3}{a^4}\right\}, \tag{20}$$

where $a'^2 = \frac{q_\perp^2}{4\alpha^2}$, $a^2 = a'^2 + 1$. Let us denote by $\mathcal{F}(q_\perp)$ the RHS of Eq. (16). The pp amplitude given by Eq. (15) then takes the form

$$T_{qq}\big(s, -\vec{q}^{\,2}\big) = \mathcal{F}(q_\perp) i\gamma_{qq} s \big(s e^{-i\frac{\pi}{2}}\big)^{\omega} \frac{1}{|t| + r_0^{-2}} \mathcal{F}(q_\perp). \tag{21}$$

Eq. (21) resembles Eq. (12). However, $\mathcal{F}(q_\perp)$ is not a form factor. It would have been the form factor $F(\vec{q}_\perp) = F(q_\perp) = \sum_{\vec{p}} \varphi^*(\vec{p} - \vec{q})\varphi(\vec{p})$, if x on the LHS of Eq. (16) were equal to 1 identically, i.e., if $\hat{s}$ were equal to s. From now on, we refer to $\mathcal{F}(q_\perp)$ as a structure factor to distinguish it from the usual form factor $F(q_\perp)$.

It is instructive to study the large momentum transfer behavior of $\mathcal{F}(q_\perp)$ and $T_{qq}(s, -\vec{q}^{\,2})$. For $a'^2 =$

$\frac{q_\perp^2}{4\alpha^2} \gg 1$ and $a^2 \simeq a'^2$, Eq. (20) yields

$$I\big(q_\perp, \alpha(x)\big) \simeq \frac{4}{q_\perp^4} \simeq \frac{4}{|t|^2} \quad \big(|t| = \vec{q}^{\,2} \simeq q_\perp^2\big). \tag{22}$$

Substituting this on the RHS of Eq. (16), we find

$$\mathcal{F}(q_\perp) \sim \frac{1}{|t|^2}. \tag{23}$$

Eq. (21) then leads to an amplitude

$$T_{qq}\big(s, -\vec{q}^{\,2}\big) \sim \frac{i\gamma_{qq} s (s e^{-i\frac{\pi}{2}})^\omega}{|t|^5}. \tag{24}$$

This results in differential cross section behavior for fixed s and large $|t|$:

$$\frac{d\sigma}{dt} \sim \frac{1}{|t|^{10}} \quad \big(s \gg |t| \gg m_0^2 + 4M^2\big). \tag{25}$$

Eq. (25) shows that we obtain the behavior predicted by the perturbative QCD dimensional counting rules [15–17] for large $|t|$.

In our pp elastic scattering model, we now have two hard-collision amplitudes: one due to ω exchange, the other due to the hard pomeron exchange. Both collisions are accompanied by cloud–cloud diffraction scattering that reduces these amplitudes by an absorption factor $\exp(i\hat{\chi}(s,0))$ [18]. So the sum of the two hard amplitudes becomes

$$T_1(s,t) = e^{i\hat{\chi}(s,0)}\left[\pm\tilde{\gamma} s \frac{F^2(t)}{m^2 - t} + i\gamma_{qq} s \big(s e^{-i\frac{\pi}{2}}\big)^\omega \frac{\mathcal{F}^2(q_\perp)}{|t| + r_0^{-2}}\right]$$
$$(+ \text{ for } \bar{p}p, - \text{ for } pp). \tag{26}$$

The first term inside the square bracket represents the ω exchange contribution; $F(t)$ is the ωNN form factor and m is the ω mass. The second term represents the hard pomeron contribution which, as stated previously, has been approximated by a fixed pole with an intercept $1+\omega$. Using the earlier parameterization [9],

$$\tilde{\gamma} e^{i\hat{\chi}(s,0)} = \hat{\gamma}_0 + \frac{\hat{\gamma}_1}{(s e^{-i\frac{\pi}{2}})^{\hat{\sigma}}}, \tag{27}$$

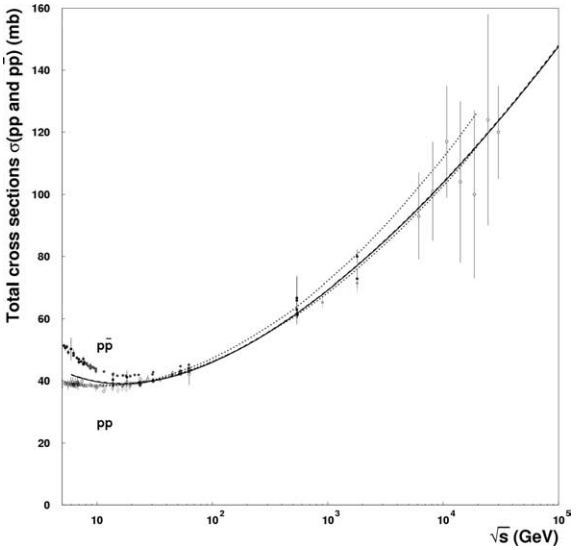

Fig. 2. Solid curve represents our calculated total cross section as a function of $\sqrt{s}$. Dotted curves represent the error band given by Cudell et al. [23].

we find

$$T_1(s,t) = \left[\hat{\gamma}_0 + \frac{\hat{\gamma}_1}{(s e^{-i\frac{\pi}{2}})^{\hat{\sigma}}}\right] \times \left[\pm s \frac{F^2(t)}{m^2 - t} + i\tilde{\gamma}_{qq} s \big(s e^{-i\frac{\pi}{2}}\big)^\omega \frac{\mathcal{F}^2(q_\perp)}{|t| + r_0^{-2}}\right], \tag{28}$$

where $\tilde{\gamma}_{qq} = \gamma_{qq}/\tilde{\gamma}$. The qq hard scattering term brings four new parameters: (i) $\tilde{\gamma}_{qq}$ which measures the relative strength of this term compared to the ω exchange term; (ii) $\alpha_{\text{BFKL}} = 1 + \omega$ which controls the high energy behavior; (iii) r_0 which provides the length scale for the black-disk radius of qq asymptotic scattering; (iv) m_0 which determines the quark wave function $\psi_0(\vec{r}) = \sqrt{\rho_0(\vec{r})}$ and the size of the quark bag. Because of the different physical aspects associated with them, these four parameters form a minimal set.

We determine the parameters of the model, which now include the hard pomeron contribution, by requiring that the model should describe satisfactorily the asymptotic behavior of $\sigma_{\text{tot}}(s)$ and $\rho(s)$ as well as the measured $\bar{p}p$ elastic $d\sigma/dt$ at $\sqrt{s} = 546$ GeV [19], 630 GeV [20], and 1.8 TeV [21,22]. The results of this investigation are shown in Figs. 2–4 together with

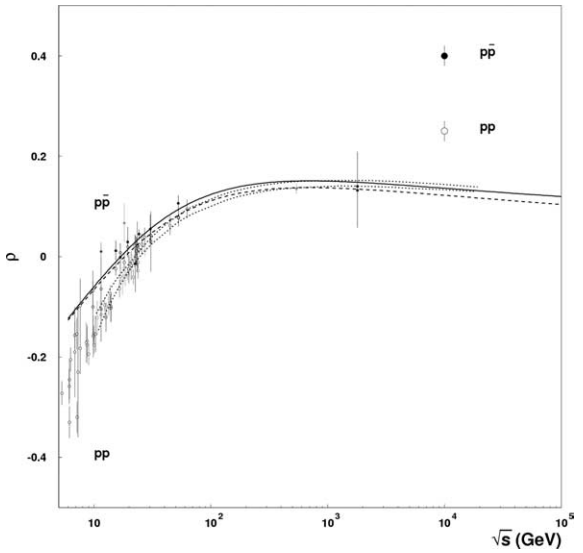

Fig. 3. Solid and dashed curves represent our calculated $\rho_{\bar{p}p}$ and ρ_{pp} as functions of $\sqrt{s}$. Dotted curves represent the error band given by Cudell et al. [23].

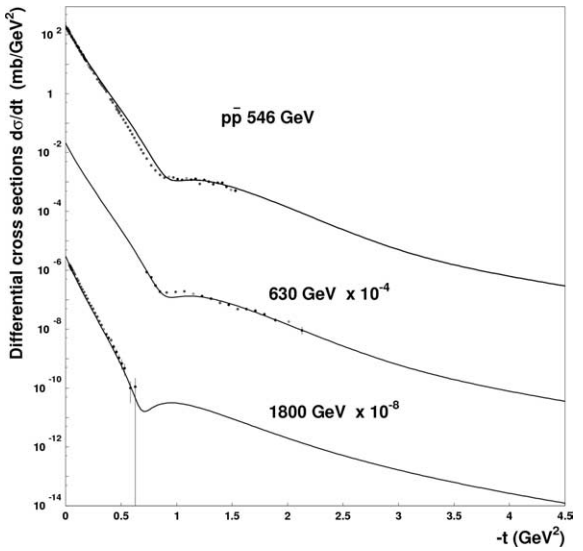

Fig. 4. Solid curves show our calculated $d\sigma/dt$ at $\sqrt{s} = 546$, 630 and 1800 GeV. Experimental data are from Refs. [19,20] and [21,22].

the experimental data. We obtain quite satisfactory descriptions. The dotted curves in Figs. 2 and 3 represent the error bands given by Cudell et al. (COMPETE Collaboration) to their best fit [23]. We notice that our $\sigma_{\text{tot}}(s)$ curve lies within their error band closer to the

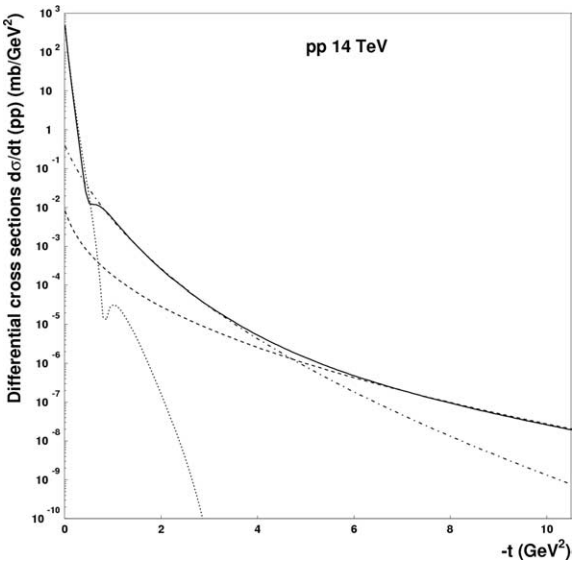

Fig. 5. Solid curve shows our predicted $d\sigma/dt$ for pp elastic scattering at $\sqrt{s} = 14$ TeV at LHC. Dotted curve represents $d\sigma/dt$ due to diffraction only. Similarly, dot-dashed curve and dashed curve represent $d\sigma/dt$ due to hard ω-exchange and hard qq scattering only.

lower curve, but our $\rho_{pp}(s)$ curve (dashed curve in Fig. 3) deviates from the band. As noted by Cudell et al., such a deviation is not surprising—since a hard pomeron occurs in our calculations and not in theirs. In fact, this hard pomeron in conjunction with a crossing-odd absorptive correction [18] in our model leads to a crossing-odd amplitude (an odderon) and produces a visible difference between $\rho_{\bar{p}p}(s)$ and $\rho_{pp}(s)$ at large $\sqrt{s}$. The parameters describing the soft (small $|t|$) diffraction amplitude and the hard (large $|t|$) ω-exchange amplitude have been discussed before [9]. Their values are: $R_0 = 2.77$, $R_1 = 0.0491$, $a_0 = 0.245$, $a_1 = 0.126$, $\eta_0 = 0.0844$, $c_0 = 0.00$, $\sigma = 2.70$, $\lambda_0 = 0.727$, $d_0 = 13.0$, $\alpha = 0.246$, $\hat{\gamma}_0 = 1.53$, $\hat{\gamma}_1 = 0.00$, $\hat{\sigma} = 1.46$ (the unit of energy is 1 GeV). The parameters β and m are kept fixed as previously: $\beta = 3.075$, $m = 0.801$. There are now seventeen adjustable parameters. The four new parameters describing the hard (large $|t|$) qq amplitude have the values $\tilde{\gamma}_{qq} = 0.03$, $\omega = 0.15$, $r_0 = 2.00$, $m_0^2 = 12.0$. (This value of m_0^2 leads to a valence quark-bag of r.m.s. radius 0.2 F, while that of the baryonic charge core is 0.44 F.) These four parameters, however, cannot be determined reliably, because no large $|t|$ elastic data are available in the TeV energy region.

Our prediction for pp elastic differential cross section at LHC at $\sqrt{s} = 14$ TeV for the whole momentum transfer range $|t| = 0$–$10\ \mathrm{GeV}^2$ is now given in Fig. 5 (solid curve). We obtain for σ_{tot} and ρ_{pp} the values 110 mb and 0.120, respectively. Also given in Fig. 5 are separate $d\sigma/dt$ due to diffraction (dotted curve), due to hard ω-exchange (dot-dashed curve), and due to hard qq scattering (dashed curve). As expected in our model, we find that in the small $|t|$ region ($|t| \simeq 0$–$0.5\ \mathrm{GeV}^2$) diffraction dominates, in the intermediate $|t|$ region ($|t| \simeq 1.0$–$4.0\ \mathrm{GeV}^2$) ω-exchange dominates, and in the large $|t|$ region ($|t| \gtrsim 6.0\ \mathrm{GeV}^2$) qq scattering dominates. The three $|t|$ regions correspond to cloud–cloud interaction, core–core scattering due to ω-exchange, and valence qq scattering via QCD hard pomeron. Therefore, they reflect the composite structure of the nucleon with an outer cloud, an inner core of topological baryonic charge, and a still smaller quark-bag of valence quarks.

We note that pp elastic differential cross section in the energy range $\sqrt{s} = 27$–62 GeV and $|t| \geqslant 3.5\ \mathrm{GeV}^2$ was observed to be approximately energy independent and falling off as t^{-8}. This was interpreted as due to the independent exchanges of three perturbative gluons [24,25]. Later it was pointed out that the three gluons would reggeize, so that color-octet exchanges would be suppressed. Instead, three color-singlet exchanges would take their place [26]. Eventually, as $|t|$ increases, a single color-singlet exchange would dominate and lead to a t^{-10} fall-off as predicted by the perturbative QCD dimensional counting rules [15–17]. In our model, the dimensional counting behavior t^{-10} of $d\sigma/dt$ originates from the hard qq amplitude in Eq. (28). This amplitude leads to a distinct change in the slope of the differential cross section from the intermediate $|t|$ region to the large $|t|$ region as seen in Fig. 5. For example, for $1.0 \leqslant |t| \leqslant 3.0\ \mathrm{GeV}^2$, $d\sigma/dt$ drops by more than two orders of magnitude, while for $7.0 \leqslant |t| \leqslant 9.0\ \mathrm{GeV}^2$, $d\sigma/dt$ drops by a factor of 4.2, i.e., less than an order of magnitude. Similar decrease in $d\sigma/dt$ slope was observed at ISR by De Kerret et al. for $|t| \gtrsim 6.5\ \mathrm{GeV}^2$ at a much lower energy: $\sqrt{s} = 53$ GeV [27]. Lepage and Brodsky [17], however, pointed out that at such low energies it would be hard to distinguish between amplitudes that lead to t^{-8} and t^{-10} asymptotic behavior.

It is interesting to note that in our model the pp elastic amplitude due to qq scattering (Eq. (21)) has $q_\perp$ dependence given by the product of two structure factors $\mathcal{F}^2(q_\perp)$ and s-dependence given by the hard-pomeron exchange (approximated by a fixed pole) with an intercept $1 + \omega$ ($\omega \simeq 0.15$). In the QCD-inspired model of Block et al. [11], the corresponding amplitude (a Born amplitude) has $q_\perp$ dependence given by the product of two dipole form factors and an s-dependence *is* that corresponds to a fixed pole of intercept 1. In the BSW model [5], the Born amplitude is again the product of two form factors, but multiplied by an additional factor, and has s-dependence given by a fixed cut: $(se^{-\frac{i\pi}{2}})^{1+c}/(\ln s - \frac{i\pi}{2})^{c'}$. Remarkably, the BSW value $1 + c = 1.167$ lies within the range given by Brodsky et al. [13]. In the last two models, multiple exchanges are considered and unitarization is done by eikonalization [14]. On the other hand, we consider a single hard-pomeron exchange modified by absorptive corrections as adequate in the TeV region we are exploring now. Typically, eikonalization leads to diffractive oscillations in $d\sigma/dt$ at LHC energy for large $|t|$ [5,7,8], whereas we obtain a smooth change from the nonperturbative regime to the perturbative regime (Fig. 5). Measurement of pp elastic $d\sigma/dt$ up to $|t| \simeq 10\ \mathrm{GeV}^2$ by the TOTEM group would therefore be able to distinguish between the eikonal models vis-à-vis our model.

We conclude: if precise measurement by the TOTEM group corroborates our predicted slow fall-off of pp elastic $d\sigma/dt$ in the large $|t|$ region, then that will provide evidence for the hard qq amplitude occurring in Eq. (28). This, in turn, will imply: (i) presence of the QCD hard pomeron, (ii) perturbative QCD dimensional counting behavior at asymptotic $|t|$ ($\gg 10\ \mathrm{GeV}^2$), and (iii) the confinement of valence quarks in a small region within the proton.

Acknowledgements

Much of this work was done when one of us (M.M.I.) was at the Yang Institute for Theoretical Physics at SUNY Stony Brook on sabbatical leave. He wishes to thank George Sterman, Director of the Institute, and other colleagues there for their hospitality. He

also wishes to thank Michael Rijssenbeek and George Sterman for stimulating discussions.

References

[1] TOTEM Collaboration, Technical Design Report, January 2004, CERN-LHCC-2004-002.
[2] A. Donnachie, H.G. Dosch, P.V. Landshoff, O. Nachtmann, Pomeron Physics and QCD, Cambridge Univ. Press, Cambridge, UK, 2002.
[3] V.A. Khoze, A.D. Martin, M.G. Ryskin, Eur. Phys. J. C 18 (2000) 167.
[4] J. Bartels, E. Gotsman, E. Levin, M. Lublinsky, U. Maor, Phys. Lett. B 556 (2003) 114.
[5] C. Bourrely, J. Soffer, T.T. Wu, Eur. Phys. J. C 28 (2003) 97.
[6] H. Cheng, T.T. Wu, Expanding Protons: Scattering at High Energies, MIT Press, Cambridge, MA, 1987.
[7] P. Desgrolard, M. Giffon, E. Matynov, E. Predazzi, Eur. Phys. J. C 16 (2000) 499.
[8] V.A. Petrov, A.V. Prokudin, Eur. Phys. J. C 23 (2002) 135.
[9] M.M. Islam, R.J. Luddy, A.V. Prokudin, Mod. Phys. Lett. A 18 (2003) 743.
[10] M.M. Islam, R.J. Luddy, A.V. Prokudin, in: Z. Parsa (Ed.), Intersections of Particle and Nuclear Physics, in: AIP Conference Proceedings, vol. 698, 2003, p. 142, hep-ph/0307355.
[11] M.M. Block, E.M. Gregores, F. Halzen, G. Pancheri, Phys. Rev. D 60 (1999) 054024;
M.M. Block, F. Halzen, T. Stanev, Phys. Rev. D 62 (2000) 077501.
[12] J.R. Forshaw, D.A. Ross, Quantum Chromodynamics and the Pomeron, Cambridge Univ. Press, Cambridge, UK, 1997.
[13] S.J. Brodsky, V.S. Fadin, V.T. Kim, L.N. Lipatov, G.B. Pivovarov, JETP Lett. 70 (1999) 155.
[14] A.B. Kaidalov, in: M. Shifman, B. Ioffe (Eds.), Regge Poles in QCD, Handbook of QCD, vol. 1, World Scientific, Singapore, 2001, p. 603.
[15] V.A. Matveev, R.M. Muradian, A.N. Tavkhelidze, Lett. Nuovo Cimento 7 (1973) 719.
[16] S.J. Brodsky, G.R. Farrar, Phys. Rev. Lett. 31 (1973) 1153;
S.J. Brodsky, G.R. Farrar, Phys. Rev. D 11 (1975) 1309.
[17] G.P. Lepage, S.J. Brodsky, Phys. Rev. D 22 (1980) 2157.
[18] M.M. Islam, B. Innocente, T. Fearnley, G. Sanguinetti, Europhys. Lett. 4 (1987) 189.
[19] M. Bozzo, et al., UA4 Collaboration, Phys. Lett. B 147 (1984) 385;
M. Bozzo, et al., UA4 Collaboration, Phys. Lett. B 155 (1985) 197.
[20] D. Bernard, et al., Phys. Lett. B 171 (1986) 142.
[21] N. Amos, et al., Phys. Lett. B 247 (1990) 127.
[22] F. Abe, et al., Phys. Rev. D 50 (1994) 5518.
[23] J.R. Cudell, et al., Phys. Rev. Lett. 89 (2002) 201801.
[24] A. Donnachie, P.V. Landshoff, Z. Phys. C 2 (1979) 55.
[25] A. Donnachie, P.V. Landshoff, Phys. Lett. B 387 (1996) 637.
[26] M.G. Sotiropoulos, G. Sterman, Nucl. Phys. B 425 (1994) 489.
[27] H. De Kerret, et al., Phys. Lett. B 68 (1977) 374.